



# Chemical adsorption of phenacyl-1,2,3-benzotriazole over $\text{AMoO}_4$ (010) scheelite surfaces. Structure and electronic properties



German Lener<sup>a,c,\*</sup>, Patricio Vélez<sup>b,\*</sup>, Ezequiel P.M. Leiva<sup>b</sup>, E. Laura Moyano<sup>c</sup>, Raúl. E. Carbonio<sup>a</sup>

<sup>a</sup> INFIQC-CONICET, Departamento de Físicoquímica, Universidad Nacional de Córdoba, Haya de la Torre esq, Medina Allende, X5000HUA Córdoba, Argentina

<sup>b</sup> INFIQC-CONICET, Departamento de Matemática y Física, Universidad Nacional de Córdoba, Haya de la Torre esq, Medina Allende, X5000HUA Córdoba, Argentina

<sup>c</sup> INFIQC-CONICET, Departamento de Química Orgánica, Universidad Nacional de Córdoba, Haya de la Torre esq, Medina Allende, X5000HUA Córdoba, Argentina

## ARTICLE INFO

### Article history:

Received 15 December 2015

Received in revised form 7 June 2016

Accepted 8 June 2016

Available online 17 June 2016

### Keywords:

Scheelite surface

Phenacyl-1,2,3-benzotriazole

Adsorption

Semiconductor interface

Catalysis

## ABSTRACT

*Ab-initio* DFT calculations are presented for the adsorption of phenacyl-1,2,3-benzotriazole on scheelite  $\text{AMoO}_4$  ( $A = \text{Ca}, \text{Sr}$  and  $\text{Ba}$ ) surfaces. Strong adsorption energy of the organic ligand on the scheelite surface is found. The formation of a bond with covalent character is due to the interaction between the high electronic density of nitrogen and oxygen atoms of the organic molecule, with the empty valence orbitals of the cationic species ( $A$ ) of the scheelite. This interaction promotes a strongly stabilized interface and it may explain the high reactivity toward nitrogen extrusion reactions in gas–solid experiments of scheelites. The energy band gap of the interface is found to decrease significantly upon molecular adsorption, indicating that this kind of adsorption could increase the conductivity of the interface.

© 2016 Elsevier B.V. All rights reserved.

## 1. Introduction

The semiconductor–organic ligand interface has been studied for various purposes and has produced important contributions in solar energy devices [1], gas-storage adsorption [2], molecular electronics [3], biosensors [4] and catalysis [5]. Many contributions have been developed by studying the electronic structure of the interface and its changes, as it is for example the case of research concerning the interaction of frontier orbitals of the organic adsorbate with the Fermi level of the surface [6–10]. Different kinds of surfaces have been considered as candidates for semiconducting interfaces; e.g. surfaces based on Silicon using different passivating substances to avoid its oxidation [11,12], which have been widely applied in technological devices. An interesting family of semiconductors is the scheelite compounds. These materials have been studied due to their local electronic levels structure [13], their scintillation properties [14,15], surface stability [16], and adsorption properties as hydrated surfaces and organic ligand interaction [17]. These materials can be obtained by various methods of synthesis such as dissolution–precipitation, ceramic method, sol–gel and microwave precipitation, among others. Through these methodologies, several numbers and types of cations can be incor-

porated in the scheelite crystal structure [18,19]. These multifunctional materials can be used with several applications that range from technological scintillators to catalysis [8,15,17–23].

Concerning the present adsorbate, benzotriazole derivatives present a number of applications at interfaces, since this organic structure and its reactivity may be used for different purposes like degradation of pollutants [24], photovoltaic structures [25], and gas–solid catalysis applied to organic synthesis [18].

With respect to computational tools applied to the present type of systems, Yu et al. have performed DFT and many-body perturbation theory calculations to study the covalent link of the thiophene molecule to Si semiconductor [26]. Thus, DFT represents an excellent computational technique to get optimized structures and reactivity of interfaces.

In a previous work, we have studied the gas–solid reaction between phenacyl-1,2,3-benzotriazole (PhBt) and scheelite oxides in catalytic flash vacuum pyrolysis experiments at 300–550 °C [18]. We have observed a strong catalytic activity and interaction between the organic ligand and the scheelite surface. The nature of this interaction, which is strongly dependent on the oxide structure, leads to the selective formation of different products.

In these experiments, we observed that the nitrogen extrusion reaction of PhBt was favored with the use of the scheelite  $\text{AMoO}_4$  catalysts, to get the azepin-7-one as the desired product or to get other products from other reaction pathways [18]. The experimental approach previously applied was the catalytic flash vacuum

\* Corresponding authors at: INFIQC-CONICET, Argentina

E-mail addresses: [germanlener@gmail.com](mailto:germanlener@gmail.com) (G. Lener), [patriciovelezromero@gmail.com](mailto:patriciovelezromero@gmail.com) (P. Vélez).

pyrolysis (cfvp) studying the reactions in the range from 300 to 550 °C. The apparatus for cfvp experiments consists of three main parts: (1) the injection region; (2) the pyrolysis region; and (3) the condensation region where products are trapped in a U-tube glass immersed in cryogenic liquids. The cfvp system was evacuated to  $1 \times 10^{-3}$  mm Hg by a high-capacity vacuum pump. A flow of carrier gas (dry N<sub>2</sub>) is regulated as 1 mL per 10 s. Under these experimental conditions, substrate molecules spend about  $1 \times 10^{-2}$  s in the hot region. The solid catalysts were placed in the middle region of the reactor, perpendicular to the trajectory of the carrier gas, using ceramic fiber as an inert support. Under these experimental conditions, the substrate PhBt afforded the nitrogen extrusion reaction of benzotriazole ring as the main transformation, at the beginning of the thermal process. Regarding these results, it can be proposed that the elimination of nitrogen could be started throughout favorable interactions between the N2 and N3 atoms of PhBt and the surface catalysts [18]. Because of this, we consider the determination of the main features on the gas–solid interaction being important. Thus, by studying the electronic structure of the adsorption geometries, it may be possible to understand the catalytic properties of scheelite catalysts in the cfvp reactions.

In the present work, we study the interaction of N2 and N3 atoms of PhBt with the scheelite slabs, considering two initial adsorption geometries: (1) PhBt (previously optimized in vacuum) with the N2 and N3 atoms on the A atom active site (see below G1 in Fig. 6) and (2) PhBt (previously optimized in vacuum) with the N2 and N3 atoms on the Mo atom in MoO<sub>4</sub> active site (see below G2 in Fig. 7). Here, for the calculation of both G1 and G2 condition, the atomic positions of the slab (previously relaxed in absence of the molecule) were fixed while a total relaxation of the PhBt molecule is allowed for the G1 and G2 condition.

To model the substrate, we consider the AMoO<sub>4</sub> (010) surface in interaction with the PhBt molecule using DFT calculations in order to analyze its electronic structure, its energetic stability and the nature of the interactions arising upon its formation. We think that these are the first steps toward the understanding of the reactivity of these interfaces.

## 2. Theory/calculation

We have used the generalized gradient approximation (GGA) in the version of Perdew–Burke–Ernzerhof (PBE) [27] to perform DFT calculations as implemented in the SIESTA code [28]. It uses Troullier–Martins norm-conserving pseudopotentials [29] to represent the nucleus and core electrons of the considered species. The basis set used for the expansion of the Kohn–Sham eigenstates is

composed of a set of numerical atomic orbitals including polarization orbitals. An energy shift of 50 meV has been chosen as a compromise between accuracy and computational efficiency. We have taken an energy cut off, of 200 Ry, and a double- $\zeta$  plus polarization orbital basis set (DZP). We use  $6 \times 6 \times 6$ -point and  $6 \times 1 \times 6$ -point for the Brillouin zone (BZ) for bulk and slab respectively. The coordinate optimization was made by conjugate gradients. All geometries have been optimized until the force on each atom was lower than 0.01 eV/Å. The crystal structure of AMoO<sub>4</sub> (A = Ca, Sr and Ba) scheelite was optimized using the atomic position and lattices parameters of the unit cell obtained experimentally by Rietveld analysis of powder X-ray diffraction [18,30] as starting structure. In gas–solid experiments, we observed a strong dependence on the reactivity of the PhBt with the A cation in the scheelite structure [18]. In order to study the energetic of the events involved in the present reaction, which occurs in the catalyst's surface, different surfaces may be considered. Flash vacuum pyrolysis experiments show that the active sites for the present reaction are provided by A-type atoms (A = Ca, Sr, Ba) [18]. For this reason we decided to cut the bulk structures in the (010) direction, thereby generating a slab which exposes the largest density of A<sup>2+</sup> cations, as compared with the (111) and (110) faces. The slab was generated by an enlargement of the y axis to 20 Å. Due to the size of PhBt, it was necessary to multiply four times the unit cell along the a lattice parameter in the x axis to ensure that the organic ligand molecules do not interact with their neighbor images (Fig. 1).

In order to analyze the surface properties we calculate the surface energy  $E_s$  as [31]

$$E_s = \frac{(E_{slab} - E_{bulk})}{2S} \quad (1)$$

where  $E_{slab}$  is the energy of the slab, which consists of one and two layers in which all atoms were relaxed (except one, to avoid translation).  $E_{bulk}$  is the energy of a piece of the bulk oxide with the same number of atoms as the slab, and  $S$  is the area of the slab. The adsorption energies of the molecule  $E_{ads}$  were as follows:

$$E_{ads} = E_{system} - (E_{slab} + E_{PhBt}) \quad (2)$$

where  $E_{system}$  is the total energy of the system,  $E_{slab}$  is the energy of the relaxed slab and  $E_{PhBt}$  is the energy of the relaxed PhBt molecule. The energy of the system was minimized allowing relaxation of all atomic coordinates of the organic ligand, while slab surface coordinates were fixed.

The pseudo charge density difference  $\Delta\eta$  is defined as follows [32]:

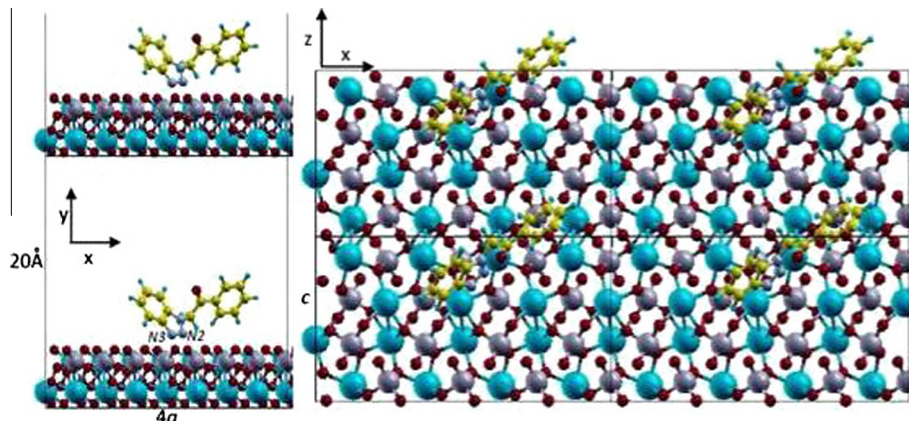


**Fig. 1.** Top and lateral view of a supercell of AMoO<sub>4</sub> (010) slab with adsorbed phenacyl-benzotriazole molecule. Spheres: C (yellow), H (light blue), N (gray), O (red), A = Ba, Ca or Sr (cyan), Mo (purple). (For interpretation of the references to color in this figure legend, the reader is referred to the web version of this article.)

$$\Delta\eta = \eta_{\text{system}} - (\eta_{\text{slab}} + \eta_{\text{PhBr}}) \quad (3)$$

where  $\eta_{\text{system}}$  is the pseudo charge density of the system,  $\eta_{\text{slab}}$  and  $\eta_{\text{PhBr}}$  are the pseudo charge density of the isolated organic ligand and scheelite slab, respectively.

The density of states (DOS) of the system and the projection onto different individual atomic orbitals (PDOS), were also calculated. The molecular graphics have been done with the XCRYSDEN package [33].

### 3. Results and discussion

#### 3.1. $\text{AMoO}_4$ ( $A = \text{Ca}, \text{Sr}$ and $\text{Ba}$ ) bulk and surfaces. Crystal and electronic structure

Powder X-ray diffraction of all synthesized  $\text{AMoO}_4$  oxides indicated that these oxides belong to the scheelite crystal structure [18]. In this structure, the  $A^{2+}$  cation has a distorted cubic coordination; whereas the  $\text{Mo}^{6+}$  cation is in the center of a slightly distorted tetrahedron forming the  $\text{MoO}_4$  species (see Fig. 2).

The space group of this structural family is the tetragonal one  $I4_1/a$ . Experimental [18] and theoretical lattices parameters and bond distances (A–O and Mo–O) for the different scheelites are shown in Table 1. The calculated values agree with the experimental data.

Fig. 3 shows the total density of states (DOS) and the projected density of states (PDOS) on the atoms of bulk  $\text{AMoO}_4$ . This figure shows the covalent character of the bond formed between atoms of Mo (4d orbital) and O atoms (2p orbital) for all scheelites considered, which compose the ionic species  $\text{MoO}_4^{2-}$ . The density of states of the A atoms shows the absence of occupied states, indicating the cationic character of this species. Mulliken population analysis indicates that the excess charge on A atoms was approximately +2, while on Mo and O was +1.15 and –0.78, respectively. The excess charge on  $\text{MoO}_4$  anionic species was, therefore, close to –2. The band gap energies  $E_G$  values calculated were 2.8, 3.0 and 3.2 eV for  $\text{CaMoO}_4$ ,  $\text{SrMoO}_4$  and  $\text{BaMoO}_4$ , respectively; indicating the bulk insulator character of these scheelites which is coincident with previous works [34–39].

The formation of (010) surface leads to the generation of a slab with O vacancies, which causes the A–O bond to be unsaturated on

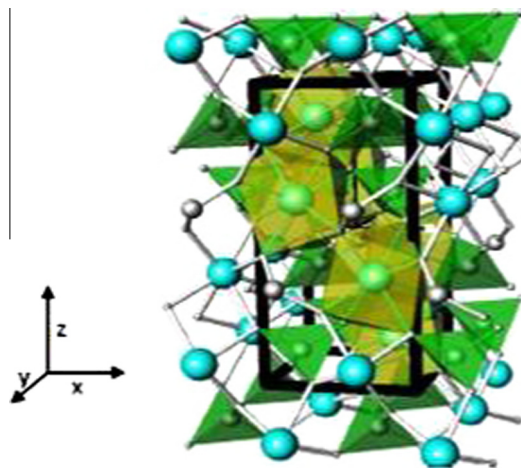


Fig. 2. Scheme of polyhedron for  $\text{AMoO}_4$  structure. Spheres: A = Ba, Ca or Sr (cyan), Mo (gray), O (white). Polyhedron:  $\text{MoO}_4$  coordination (green),  $\text{AO}_8$  coordination (yellow). (For interpretation of the references to color in this figure legend, the reader is referred to the web version of this article.)

Table 1

Average distances of cation-oxygen, and lattices parameters in molibdates.

Solid	Lattice parameters		Atomic distances					
	a, c <sup>a</sup>	a, c <sup>b</sup>	A–O <sup>a</sup>	Mo–O <sup>a</sup>	A–O <sup>b</sup>	Mo–O <sup>b</sup>	A–O <sup>c</sup>	Mo–O <sup>c</sup>
$\text{CaMoO}_4$	5.1, 11.1	5.3, 11.9	2.46	1.76	2.50	1.79	2.44	1.71
$\text{SrMoO}_4$	5.4, 12.1	5.4, 12.2	2.63	1.71	2.58	1.77	2.47	1.78
$\text{BaMoO}_4$	5.6, 12.8	5.7, 13.6	2.75	1.78	2.90	1.77	2.80	1.74

Lattices parameters and atomic distances in Å for:

<sup>a</sup> Experimental DRX and Rietveld analysis.

<sup>b</sup> DFT of bulk.

<sup>c</sup> DFT of slab.

the surface. This situation provokes changes in the geometry and in the electronic structure compared to the bulk. Geometric differences can be observed in Table 1. In the bulk, the cationic species A is coordinated by eight O atoms ( $\text{AO}_8$ ), while in the slab, the cleavage of A–O bond decreases the coordination number to 5

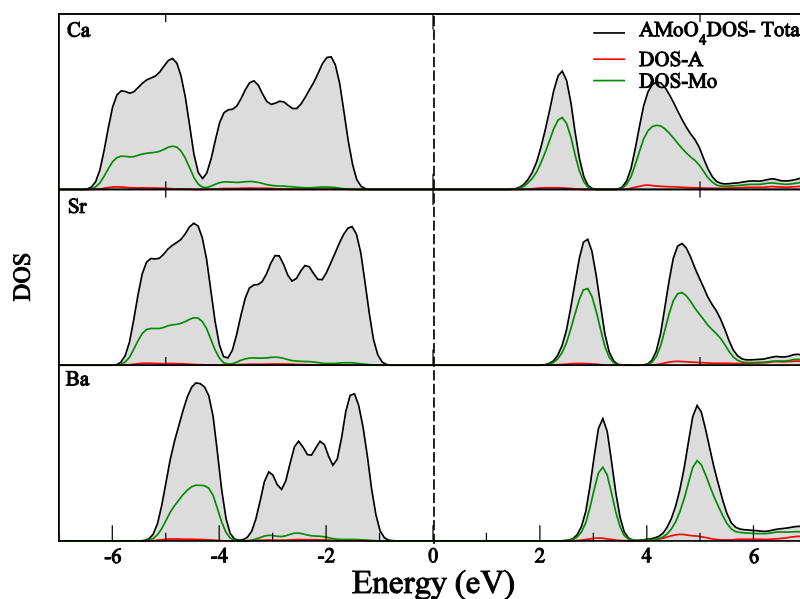
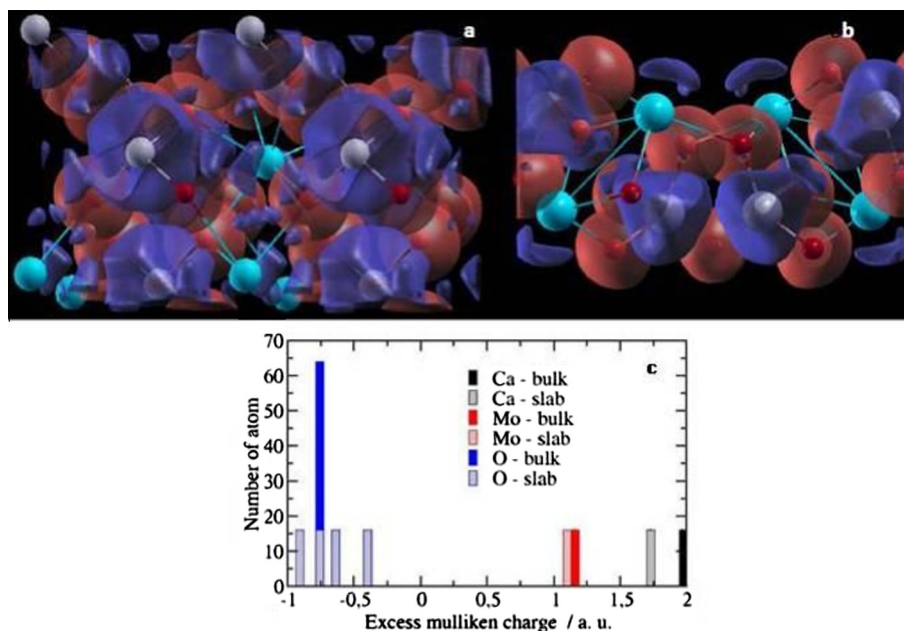
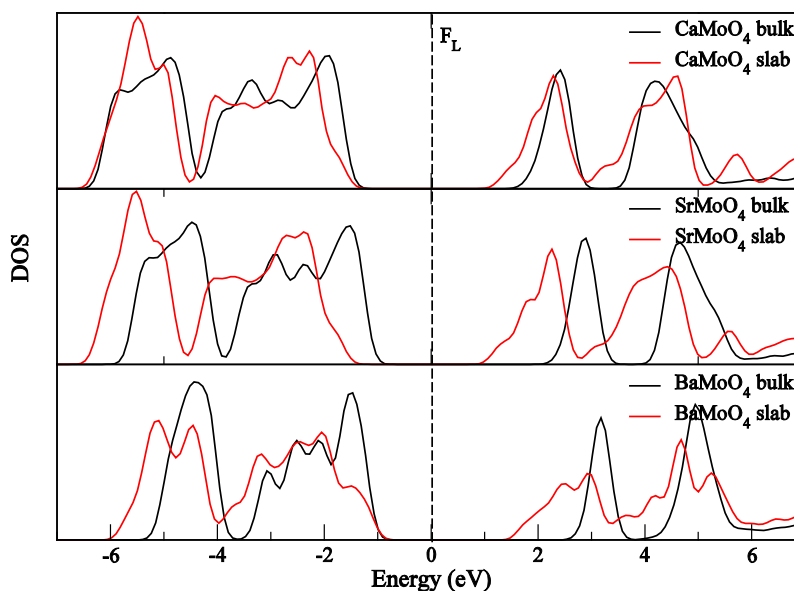


Fig. 3. Density of states (DOS) for  $\text{AMoO}_4$  ( $A = \text{Ca}, \text{Sr}$  and  $\text{Ba}$ ).



**Fig. 4.** Pseudo differential density of charge for: (a) bulk and (b) slab of CaMoO<sub>4</sub>. The blue isosurface indicates depletion of charge, the red isosurface indicates accumulation of charge. Density of charge at the isosurface: 0.005 e/Bohr<sup>3</sup>. Spheres: Ca (cyan), Mo (purple), O (red). (c) Distribution of excess of Mulliken charge over atoms in bulk and slab for CaMoO<sub>4</sub> scheelite. (For interpretation of the references to color in this figure legend, the reader is referred to the web version of this article.)



**Fig. 5.** Comparative density of states (DOS) for bulk and slab of AMoO<sub>4</sub> (A = Ca, Sr, Ba).

(AO<sub>5</sub>), forming a distorted square pyramidal geometry after relaxation of the slab. This decrease in coordination number needs to be compensated by a decrease in the bond distances in A–O (see Table 1). Another important aspect in the square pyramidal coordination (AO<sub>5</sub>) in the slab is the O–A–O bond angle between the oxygen atoms of the plane and the atom at the tip of the pyramid. This angle varies as a function of the A cation radii and their values are 85.2°, 78.0° and 76.8° for Ca, Sr and Ba, respectively. This indicates that the larger the cation radius is, the higher the distortion of the A environment in the slab results. On the other hand, the tetrahedron formed between Mo and O atoms (MoO<sub>4</sub>), practically does not change. Thus, the Mo–O bond distances and O–Mo–O bond angles when the slab (010) did not change significantly in comparison with the bulk. The electronic differences between the bulk and slab

are shown in Figs. 4 and 5. In Fig. 4a and b we can observe the differential pseudo charge density for CaMoO<sub>4</sub> bulk and slab. It can be

**Table 2**  
Surface properties of bulk and slab in the scheelite systems.

Solid	$E_S$ 1×1×1	$E_S$ 1×2×1	$E_G$ bulk	$E_G$ slab <sup>a</sup>	$Q_{\text{Mulliken}}$ A bulk	$Q_{\text{Mulliken}}$ A slab <sup>a</sup>
CaMoO <sub>4</sub>	0.96	1.11	2.8	1.9	1.86+	1.66+
SrMoO <sub>4</sub>	1.12	1.13	3.0	1.9	1.85+	1.72+
BaMoO <sub>4</sub>	0.80	0.89	3.2	1.7	1.81+	1.78+

$E_S$ : surface energy (J/m<sup>2</sup>),  $E_G$ : energy of the band gap (eV),  $Q_{\text{Mulliken}}$ : charge from Mulliken population analysis.

<sup>a</sup>  $E_G$  and  $Q_{\text{Mulliken}}$  values correspond to the 1 × 1 × 1 slab.

see that the depletion of charge density (blue contour) surrounding Ca site atom decrease in the slab formation respects to the bulk due to the unsaturated atoms. Fig. 4c shows the Mulliken excess charge per atom for both, the bulk and the slab of  $\text{CaMoO}_4$ . Here we can see how the oxygen atoms have different excess charge because some are more exposed to the surface while others remain

**Table 3**

Energy of adsorption and energy of band gap for PhBt adsorbed on the scheelite surface for G1 and G2 geometries.

Solid	$E_{\text{ads}} \text{ G1}$ (kJ/mol)	$E_{\text{ads}} \text{ G2}$ (kJ/mol)	$E_{\text{gap}} \text{ G1}$ (eV)	$E_{\text{gap}} \text{ G2}$ (eV)
$\text{CaMoO}_4$	-172	-284	1.5	0.3
$\text{SrMoO}_4$	-235	-288	1.2	0.2
$\text{BaMoO}_4$	-238	-242	0.5	0

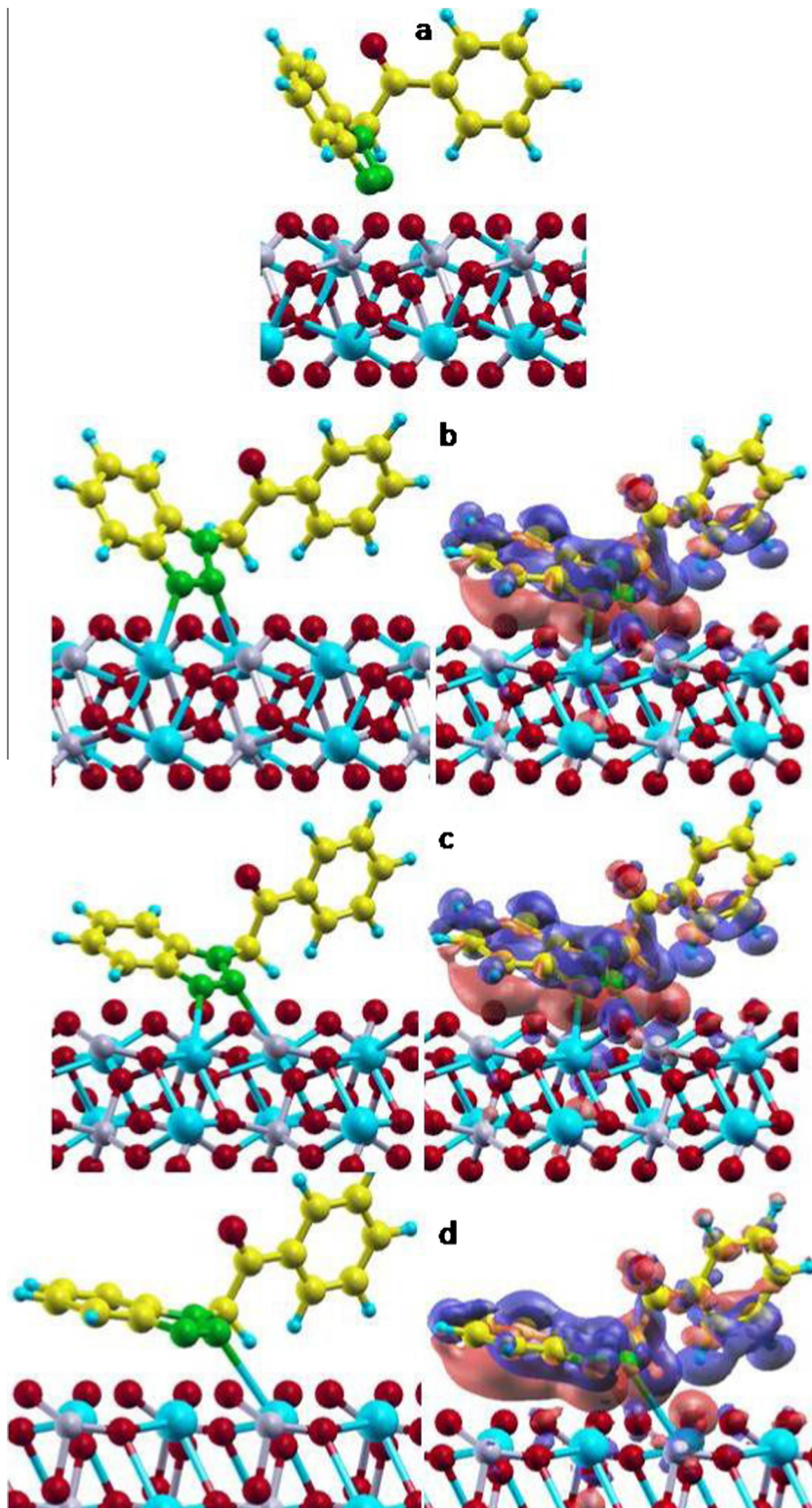


**Fig. 6.** G1 condition: (a) Initial geometry of adsorption for PhBt on  $\text{AMoO}_4$  surface. (b, c, d) Relaxed geometries and pseudo differential density of charge for  $\text{CaMoO}_4$ ,  $\text{SrMoO}_4$  and  $\text{BaMoO}_4$ , respectively. Red isosurface: accumulation of charge, blue isosurface: depletion of charge. Isosurface value: 0.005  $e/\text{Bohr}^3$ . Spheres: A = Ca, Sr, Ba (cyan), Mo (purple), O (red), N (green), C (yellow), H (light blue). (For interpretation of the references to color in this figure legend, the reader is referred to the web version of this article.)

better coordinated internally. We find the same trend for  $\text{SrMoO}_4$  and  $\text{BaMoO}_4$  scheelites.

Fig. 5 shows the DOS of the  $\text{AMoO}_4$  bulk and slab. The generation of electronic virtual states close to the conduction band can be seen, as a consequence of the unsaturated bond A–O. This defect makes that the band-gap energies of the slab decrease with respect

to the bulk ones. This effect was more prominent for  $\text{BaMoO}_4$  than for  $\text{SrMoO}_4$  and  $\text{CaMoO}_4$ .

Table 2 shows the band gap energies and the surface energy for these slabs. The surface energies were similar to those reported by other authors for similar systems [16,38]. The band gap energies for these slabs were 1.9, 1.9 and 1.7 eV for  $\text{CaMoO}_4$ ,  $\text{SrMoO}_4$  and

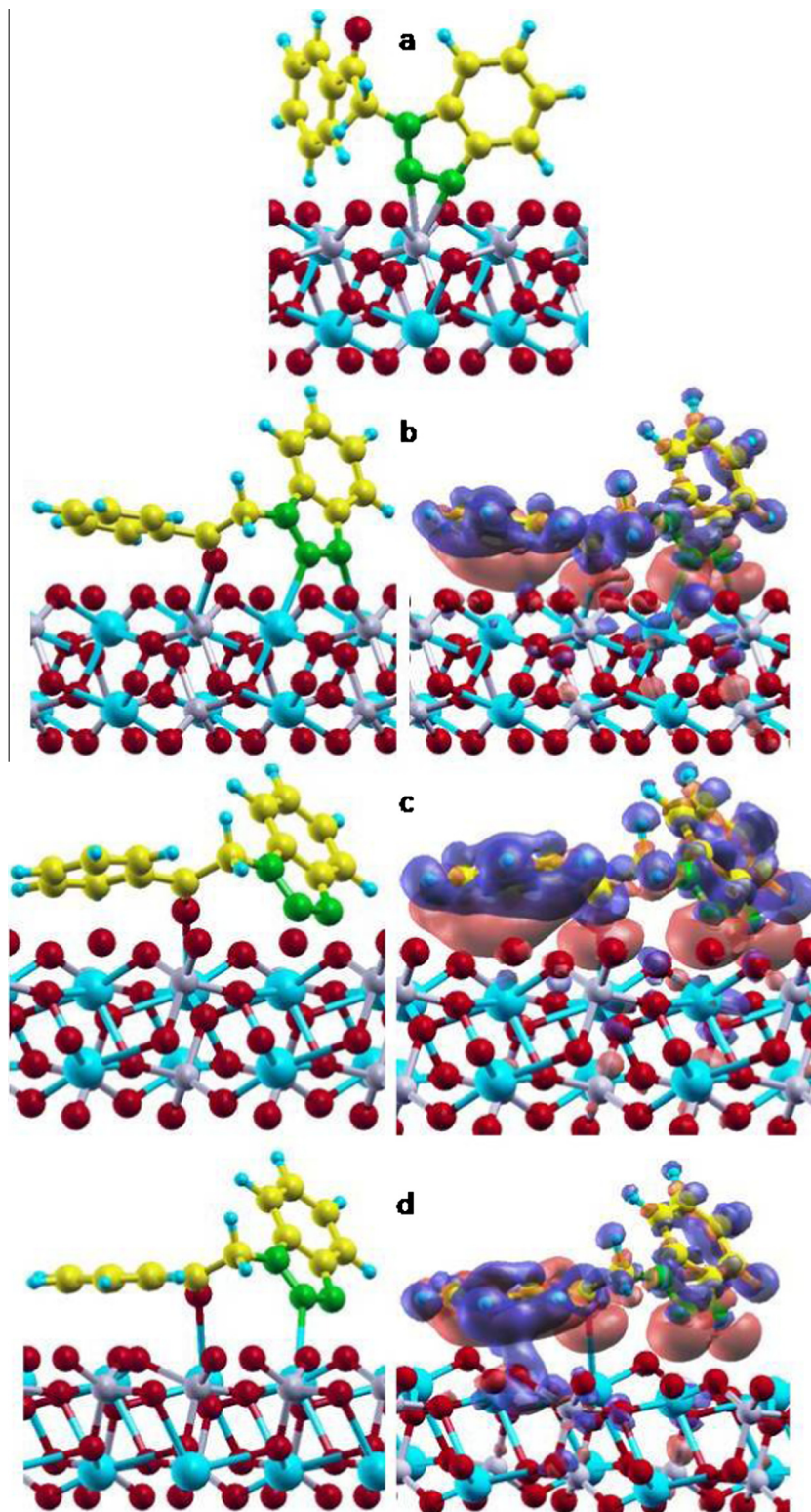


**Fig. 7.** G2 condition: (a) initial geometry of adsorption for PhBt on  $\text{AMoO}_4$  surface. (b, c, d) Relaxed geometries and pseudo differential density of charge for  $\text{CaMoO}_4$ ,  $\text{SrMoO}_4$  and  $\text{BaMoO}_4$ , respectively. Red isosurface: accumulation of charge, blue isosurface: depletion of charge. Isosurface value:  $0.005 \text{ e/Bohr}^3$ . Spheres: A = Ca, Sr, Ba (cyan), Mo (purple), O (red), N (green), C (yellow), H (light blue). (For interpretation of the references to color in this figure legend, the reader is referred to the web version of this article.)

BaMoO<sub>4</sub>, respectively; which indicates that these defects make surfaces more conducting.

### 3.2. Energetic, geometries and electronics structure of the adsorption of phenacyl-1,2,3-benzotriazole on the AMoO<sub>4</sub> surface

Once the geometry of the PhBt molecule was optimized in vacuum, the molecule was oriented with the nitrogen atoms (N2 and N3) pointing toward the surface of AMoO<sub>4</sub>.

Before placing the organic molecule on the scheelite surface, we evaluated the influence of the slab thickness on the value of surface energy. As mentioned before, due to the size of the molecule, each unit cell has 96 atoms in its thinnest slab, and by adding an additional sheet the solid increments its number of atoms to 192, leading the system to a total of 221 atoms (slab and molecule). However, it should be bear in mind that this growth of the surface thickness generates a significant increase in computational time, without an important change in the calculated surface energies, as it is shown in Table 2. Because of this, we used the thinnest slab in all the calculations of the organic heterocycle adsorbed on the scheelite surface.

As mentioned above, in order to avoid the interaction between neighboring molecules in the *x*-*z* plane, the unit cell was increased four times in the direction *x*, thus, the surface contains 96 atoms. In this way, the spacing between molecules was about 10 Å.

Fig. 6a shows the initial geometry of PhBt molecule adsorbed on the A atoms and the Fig. 6b–d shows the relaxed geometries, for A = Ca, Sr and Ba respectively. The adsorption energies found for the optimized final geometry of the G1 condition were: –171.8, –235.3 and –237.8 kJ/mol for CaMoO<sub>4</sub>, SrMoO<sub>4</sub> and BaMoO<sub>4</sub>, respectively (see Table 3).

These high exothermic energies are an indication the formation of a covalent bond character between the organic molecule and the slab of scheelite. From an electronic point of view, it is noteworthy that the pseudo differential charge density presents an accumulation of charge between the N2 and N3 atoms of PhBt and the

cationic species A. Charge accumulation is also observed between the heterocyclic ring of the molecule and the slab of scheelite (particularly for A = Sr and Ba) (see Fig. 6b–d). Another interesting aspect to remark was the decrease of the band gap ( $E_G$ ) of the systems G1 compared to the clean surface of scheelites (see Table 3).

For the G2 condition, Fig. 7a shows the initial geometry of PhBt molecule adsorbed on the Mo atoms. The optimization of geometry, as shown in Fig. 7b–d, locates the N2, N3 and O atoms of the molecule in the vicinity of the A atoms of the scheelites (similar to the final geometry of the G1 condition).

The adsorption energy values found for the geometries of the G2 condition were: –284, –288 and –242 kJ/mol to CaMoO<sub>4</sub>, SrMoO<sub>4</sub> and BaMoO<sub>4</sub>, respectively (see Table 3). The interaction of the cationic species A with the O atom of the PhBt molecule makes these energies more stable than those found for the geometries of the G1 condition. The energetic stabilization is more remarkable for systems with scheelites of CaMoO<sub>4</sub> and SrMoO<sub>4</sub>.

Fig. 7b–d also shows the *pseudo* differential charge density for the G2 condition. In all cases, we obtained a charge accumulation between N2, N3 and O atoms of PhBt and the A atom of the scheelites. The accumulation of charge between the atoms is higher for the CaMoO<sub>4</sub> and SrMoO<sub>4</sub> systems, something which is consistent with the most stable energy values found for those systems.

An important aspect in the adsorption properties was the significant decrease in the band gap energies of the surfaces to 0.3, 0.2 and 0.0 eV for CaMoO<sub>4</sub>, SrMoO<sub>4</sub> and BaMoO<sub>4</sub>, respectively (Table 3). These results suggest that this kind of adsorption could cause an increase of the conductance of the interface with respect to the clean surface.

Fig. 8a–c shows the density of states of the atoms involved in the formation of chemical bonds between the surface and the organic-ligand for A = Ca, Sr and Ba respectively. We can appreciate the overlap of the high density of states of the N2, N3 and O atoms of PhBt with the low density of states of the A cationic species in the valence band. This finding suggests that the nitrogen and oxygen atoms of the organic molecule contribute with electronic

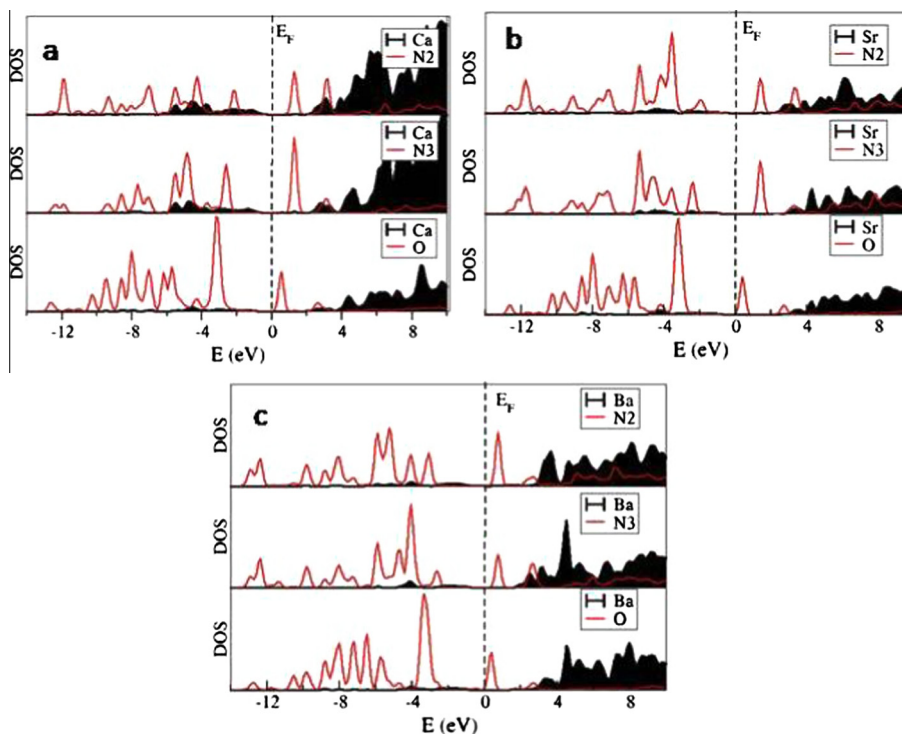


Fig. 8. Density of states (DOS) projected onto atoms involved in the chemical superficial bond for the relaxed geometries of the G2 condition.

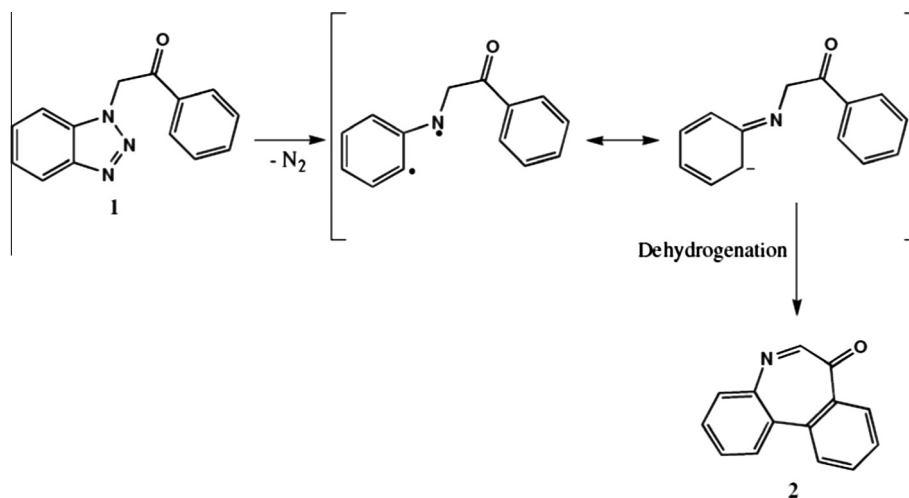


Fig. 9. Scheme of the formation of dibenzo-azepinone (2) from phenacyl-benzotriazole (1).

density and the A cationic specie contributes with empty valence orbitals to generate a strong interaction at the interface. This acceptor–donor character results in high adsorption energies, the formation of covalent bonds character and important changes in the electronics structure of the system.

From a catalytic point of view and compared with the experimental results [18], the thermal process addressed in the introduction probably starts with a nitrogen extrusion of the organic molecule assisted by the A cationic species. The values of the adsorption energies from DFT indicate a strongly bond. The desorption process is probably activated, however, the experimental conditions (temperature, low pressure and flow) could assist N<sub>2</sub> extrusion generating total conversion at 150–200 °C lower than the un-catalyzed reactions. This experimental result indicates a significant increase in the activity of the catalyzed system. Thereby, it is possible that the G1 and G2 geometries may be the starting structures and thus, the PhBt molecule could explore an alternative pathway of reaction with low activation energy. Then, it may be efficiently converted into different products of reaction. The products of the reaction involve a nitrogen extrusion to generate a carbene as intermediated of reaction and thereafter the dehydrogenation and cyclization leads to the formation of the desired azepinone (Fig. 9) [18]. The nitrogen extrusion can be performed thought the interaction between N2–N3 atoms of PhBt and the A<sup>2+</sup> cation of surface. Moreover, it probably that the interaction between the oxygen atoms of the molecule and the A<sup>2+</sup> cation in G2 geometry provide the cyclization PhBt to generate the desired structure with an great efficient respect to the uncatalyzed system.

#### 4. Conclusion

The chemical interaction of phenacyl-1,2,3-benzotriazole with AMoO<sub>4</sub> scheelite surfaces was studied using theoretical calculations to understand the main properties of this interface. For this purpose, slabs of AMoO<sub>4</sub> (A = Ca, Sr, Ba) that exhibit the (010) face were generated from the bulk material. The adsorption of the organic-ligand on the AMoO<sub>4</sub> slab was found to be strongly exothermic. The analysis of the projected density of states indicates that the strong interaction energy between the organic molecule and the scheelite surface is due to the formation of covalent bonds between the N2, N3 and O atoms of the organic molecule and the A atoms of the scheelite slabs. Occupied states of the N2, N3 and O atoms are found to overlap with empty states of A cationic species of the scheelite. The properties of these chemical bonds,

occurring at the interface PhBt/AMoO<sub>4</sub>, indicate that these surfaces may be useful for different purposes. On the one hand, the can be used as catalysts for *cfvp* systems, where the A cationic species site can strongly interact with electronegative atoms of the gas molecule. Thus, the thermal experimental conditions would favor desorption of the reactive intermediate from the catalyst's surface to form different products. On the other hand, the interaction can be used to generate surfaces with semiconducting/conducting properties, because the slab showed a decrease in the band gap energy respect to the bulk upon molecular adsorption. This could be used with sensing applications.

#### Acknowledgments

This work was supported by grants PIP-11220110100992, FonCyT PICT-2010-2324, SECyT Universidad Nacional de Córdoba (Argentina), CCAD-UNC and GPGPU Computing Group.

#### References

- [1] Y. Li, L.E.O. Leary, N.S. Lewis, G. Galli, Combined theoretical and experimental study of band-edge control, *J. Phys. Chem. C* 117 (2013) 5188–5194.
- [2] H. Wang, X. Yuan, Y. Wu, H. Huang, X. Peng, G. Zeng, H. Zhong, J. Liang, M. Ren, Graphene-based materials: fabrication, characterization and application for the decontamination of wastewater and wastegas and hydrogen storage/generation, *Adv. Colloid Interface Sci.* 195–196 (2013) 19–40.
- [3] M. Scarrozza, G. Pourtois, M. Houssa, M. Caymax, A. Stesmans, M. Meuris, M.M. Heyns, A first-principles study of the structural and electronic properties of III–V/thermal oxide interfaces, *Microelectron. Eng.* 86 (2009) 1747–1750.
- [4] Z. Chen, X. Ren, X. Meng, L. Tan, D. Chen, F. Tang, Quantum dots-based fluorescent probes for turn-on and turn-off sensing of butyrylcholinesterase, *Biosens. Bioelectron.* 44 (2013) 204–209.
- [5] A.M. Munshi, D.L. Dheeraj, J. Todorovic, A.T.J. van Helvoort, H. Weman, B.O. Fimland, Crystal phase engineering in self-catalyzed GaAs and GaAs/GaAsSb nanowires grown on Si(111), *J. Cryst. Growth* 372 (2013) 163–169.
- [6] S. Shalabi, M. El Mahdy, H.O. Taha, Screening of thiophene-substituted metalloporphyrins (Zn, Ni, Fe, Ti) for use in dye-sensitized solar cells DFT and TD-DFT study, *J. Nanoparticle Res.* 15 (2013) 1–16.
- [7] N. Saikia, R.C. Deka, A comparison of the effect of nanotube chirality and electronic properties on the  $\pi$ – $\pi$  interaction of single-wall carbon nanotubes with pyrazinamide antitubercular drug, *Int. J. Quantum Chem.* 113 (2013) 1272–1284.
- [8] O. Yaffe, Y. Qi, L. Scheres, S.R. Puniredd, L. Segev, T. Ely, H. Haick, H. Zuilhof, A. Vilan, L. Kronik, A. Kahn, et al., Charge transport across metal/molecular (alkyl) monolayer-Si junctions is dominated by the LUMO level, *Phys. Rev. B* 85 (2012) 1–8.
- [9] G. Wang, Y. Kim, S.I. Na, Y.H. Kahng, J. Ku, S. Park, Y.H. Jang, D.Y. Kim, T. Lee, Investigation of the transition voltage spectra of molecular junctions considering frontier molecular orbitals and the asymmetric coupling effect, *J. Phys. Chem. C* 115 (2011) 17979–17985.

- [10] L. Kong, F. Chesneau, Z. Zhang, F. Staier, A. Terfort, P.A. Dowben, M. Zharnikov, Electronic structure of aromatic monomolecular films: the effect of molecular spacers and interfacial dipoles, *J. Phys. Chem. C* 115 (2011) 22422–22428.
- [11] M.F. Juarez, F.A. Soria, E.M. Patrito, P. Paredes-Olivera, The role of the organic layer functionalization in the formation of silicon/organic layer/metal junctions with coinage metals, *Phys. Chem. Chem. Phys.* 13 (2011) 21411–21422.
- [12] F.A. Soria, E.M. Patrito, P. Paredes-Olivera, Oxidation of hydrogenated Si(111) by a radical propagation mechanism, *J. Phys. Chem. C* 116 (2012) 24607–24615.
- [13] J.C. Conesa, Computer modeling of local level structures in (Ce, Zr) mixed oxide, *J. Phys. Chem. B* 107 (2003) 8840–8853.
- [14] L.S. Cavalcante, V.M. Longo, J.C. Sczancoski, M.A.P. Almeida, A. Batista, J.A. Varela, M.O. Orlandi, E. Longo, M.S. Li, Electronic structure, growth mechanism and photoluminescence of  $\text{CaWO}_4$  crystals, *CrystEngComm* 14 (2012) 853–868.
- [15] G. Angloher, C. Bucci, C. Cozzini, F. von Feilitzsch, T. Frank, D. Hauff, S. Henry, T. Jagemann, J. Jochum, H. Kraus, et al., Cresst-II: dark matter search with scintillating absorbers, *Nucl. Instrum. Methods Phys. Res. Sect. A: Accel. Spectrom., Detect. Assoc. Equip.* 520 (2004) 108–111.
- [16] Y. Hu, Z. Gao, W. Sun, X. Liu, Anisotropic surface energies and adsorption behaviors of scheelite crystal, *Colloids Surf. A: Physicochem. Eng. Aspects* 415 (2012) 439–448.
- [17] T.G. Cooper, N.H. de Leeuw, A combined Ab initio and atomistic simulation study of the surface and interfacial structures and energies of hydrated scheelite: introducing a  $\text{CaWO}_4$  potential model, *Surf. Sci.* 531 (2003) 159–176.
- [18] G. Lener, R.E. Carbonio, E.L. Moyano, Mixed oxides as highly selective catalysts for the flash pyrolysis of phenacyl benzotriazole: one-pot synthesis of dibenzazepin-7-one, *ACS Catal.* 3 (2013) 1020–1025.
- [19] J.T. Klopogge, M.L. Weier, L.V. Duong, R.L. Frost, Microwave-assisted synthesis and characterisation of divalent metal tungstate nanocrystalline minerals: ferberite, hübnerite, sanmartinite, scheelite and stolzite, *Mater. Chem. Phys.* 88 (2004) 438–443.
- [20] H. Lei, X. Zhu, Y. Sun, W. Song, Preparation of  $\text{SrMoO}_4$  thin films on Si substrates by chemical solution deposition, *J. Cryst. Growth* 310 (2008) 789–793.
- [21] V.B. Mikhailik, H. Kraus, D. Wahl, M.S. Mykhaylyk, Studies of electronic excitations in  $\text{MgMoO}_4$ ,  $\text{CaMoO}_4$  and  $\text{CdMoO}_4$  crystals using VUV synchrotron radiation, *Phys. Status Solidi* 242 (2005) 17–19.
- [22] V.B. Mikhailik, S. Henry, H. Kraus, I. Solskii, Temperature dependence of  $\text{CaMoO}_4$  scintillation properties, *Nucl. Instrum. Methods Phys. Res. Sect. A: Accel. Spectrometers, Detect. Assoc. Equip.* 583 (2007) 350–355.
- [23] V. Mikhailik, H. Kraus, S. Henry, A. Tolhurst, Scintillation studies of  $\text{CaWO}_4$  in the millikelvin temperature range, *Phys. Rev. B* 75 (2007) 1–6.
- [24] D.B. Mawhinney, B.J. Vanderford, S.A. Snyder, Transformation of 1H-benzotriazole by ozone in aqueous solution, *Environ. Sci. Technol.* 46 (2012) 7102–7111.
- [25] F.M. Pasker, M.F.G. Klein, M. Sanyal, E. Barrera, U. Lemmer, A. Colmann, S. Höger, Photovoltaic response to structural modifications on a series of conjugated polymers based on 2-aryl-2H-benzotriazoles, *J. Polym. Sci. Part A: Polym. Chem.* 49 (2011) 5001–5011.
- [26] M. Yu, P. Doak, I. Tamblyn, J.B. Neaton, Theory of covalent adsorbate frontier orbital energies on functionalized light-absorbing semiconductor surfaces, *J. Phys. Chem. Lett.* 4 (2013) 1701–1706.
- [27] J. Perdew, K. Burke, M. Ernzerhof, Generalized gradient approximation made simple, *Phys. Rev. Lett.* 77 (1996) 3865–3868.
- [28] M. Soler, E. Artacho, J.D. Gale, A. Garcia, J. Junquera, P. Ordej, S. Daniel, The SIESTA method for ab initio order-N materials, *J. Phys.: Condens. Matter* 14 (2002) 2745–2779.
- [29] N. Troullier, J.L. Martins, Efficient pseudopotentials for plane-wave calculations. II. Operators for fast iterative diagonalization, *Phys. Rev. B* 43 (1991) 8861–8869.
- [30] H. Rietveld, Rietveld method a historical perspective, *Aust. J. Phys.* 41 (1988) 113–116.
- [31] A. Arya, E.A. Carter, Structure, bonding, and adhesion at the  $\text{ZrC}(100)/\text{Fe}(110)$  interface from first principles, *Surf. Sci.* 560 (2004) 103–120.
- [32] A. Kokalj, A. Dal Corso, S. de Gironcoli, S. Baroni, The interaction of ethylene with perfect and defective  $\text{Ag}(001)$  surfaces, *J. Phys. Chem. B* 106 (2002) 9839–9846.
- [33] A. Kokalj, Computer graphics and graphical user interfaces as tools in simulations of matter at the atomic scale, *Comput. Mater. Sci.* 28 (2003) 155–168.
- [34] S.K. Sharma, S. Dutta, S. Som, P.S. Mandal,  $\text{CaMoO}_4:\text{Dy}^{3+}$ ,  $\text{K}^+$  near white light emitting phosphor: structural, optical and dielectric properties, *J. Mater. Sci. Technol.* 29 (2013) 633–638.
- [35] J.C. Sczancoski, L.S. Cavalcante, M.R. Joya, J.W.M. Espinosa, P.S. Pizani, J.A. Varela, E. Longo, Synthesis, growth process and photoluminescence properties of  $\text{SrWO}_4$  powders, *J. Colloid Interface Sci.* 330 (2009) 227–236.
- [36] J.C. Sczancoski, L.S. Cavalcante, N.L. Marana, R.O. da Silva, R.L. Tranquilin, M.R. Joya, P.S. Pizani, J.A. Varela, J.R. Sambrano, M. Siu Li, et al., Electronic structure and optical properties of  $\text{BaMoO}_4$  powders, *Curr. Appl. Phys.* 10 (2010) 614–624.
- [37] T. Yamamoto, T. Mizoguchi, First principles study on oxygen vacancy formation in rock salt-type oxides MO (M: Mg, Ca, Sr and Ba), *Ceram. Int.* 39 (2013) S287–S292.
- [38] T.G. Cooper, N.H. de Leeuw, A computer modeling study of the competitive adsorption of water and organic surfactants at surfaces of the mineral scheelite, *Langmuir* 20 (2004) 3984–3994.
- [39] Y. Zhang, N.A.W. Holzwarth, R.T. Williams, Electronic band structures of the scheelite materials  $\text{CaMoO}_4$ ,  $\text{CaWO}_4$ ,  $\text{PbMoO}_4$ , and  $\text{PbWO}_4$ , *Phys. Rev. B* 57 (12) (2004) 738–750.